VISIONLESS TRAC

A FINAL REPORT
FOR PROJECT
NAG 9-549; Basic

Prepared for: Leo Monford, NASA-JSC

by
Louis J. Everett
Texas A&M University

September 10, 1992

CONTENTS

ABSTRACT

This final report documents the activities during a sabbatical. Leo Monford of JSC was the principal NASA contact for this work. The work performed supported Mr. Monford's activities in several projects. As a result, this report discusses several seeming disjoint projects.

Approximately 5 months were spent with Mr. Monford in the New Initiatives Office at JSC. During this time the work supported a flight experiment planned by the Space Research Consortium of ERIM in Michigan. The work investigated the potential of using a TRAC sensor to autonomously rendezvous satellites.

Other work at the NIO supported the Explorer flight experiment by providing TRAC reflectors for future rendezvous experiments.

The third major project initiated at the NIO was a visionless TRAC sensing concept called the PSD concept. The PSD project contains some new, perhaps patentable, technology therefore it will not be extensively documented in this report.

For the remaining 4 months of the sabbatical Mr. Monford was working in the Automation and Robotics branch at JSC. Major projects performed at the A&R included demonstrating autograpple technology, and development of the PSD concept.

SUPPORT OF SPARC'S SATELLITE RENDEZVOUS

This section describes the support provided for an experiment on autonomous rendezvous of satellites. Most of the work was performed in the New Initiatives Office.

This section describes a TRAC (Targeting Reflective Alignment Concept) based sensing system for use in an autonomous rendezvous and docking experiment. The proposed experiment will utilize a COMET (COMmercial Experiment Transporter) based target satellite and a second chase vehicle. The sensor system consists of a target mounted on the target vehicle and a vision based sensor on the chase vehicle. The target has both active and passive components to enable the evaluation of both technologies. The chase vehicle will possess structured lighting and a single off the shelf camera.

Lighting will be provided by several strategically placed "kilo-bright" LEDs capable of emitting 2500 millicandela with 40 milliwatts of input. The structured lighting will be used to eliminate background illumination caused by earth shine and solar glare. The proposed CCD camera will utilize a fixed focal length, fixed iris lens and a bandpass filter tuned to the LED wavelength. Complex vision processing can be avoided using the structured lights, therefore data is expected to be obtained at a rate of several cycles per second.

Preliminary tests indicate the targeting system is capable of providing data from 1 meter to 300 meters range.

Parameter	Value
Orbit	300 nmi, 40 degree incl
Attitude Pointing	$\pm 1^{\circ}$
Available Power	350 Watts Cont.
Communications	
- Commands	9600 Baud
- Data	250 kBaud
- Transmission Time	5 pass/day, 40 min/day
Thrust	20 lb Cold Gas
Weight	1000 lb

Table 1: Basic Experiment Parameters.

Introduction

This paper describes support for an Autonomous Rendezvous and Docking experiment [1]. The experiment will occur in the 1994 timeframe and will utilize two expendable launch vehicles (COMETs). The key objectives of the experiment are to demonstrate cost-effective resupply capability with a cooperative target. The specific support consists of the design of a six degree of freedom targeting sensor constructed from commercially available components.

The sensing system studied and reported on is an autonomous version of the Tracking and Reflective Alignment Sensor (TRAC) [2]. The TRAC system was chosen for three reasons: (1) an autonomous version was recently demonstrated to be robust and accurate, (2) it has excellent orientation measurement resolution, and (3) it is cost effective. The TRAC system itself will be described in detail in a later subsection.

Some basic mission parameters are given in Table 1. To reduce cost and complexity a few restrictions have been placed on the system design. For example, we hope to perform ARD via a single, fixed iris camera lense. The chase vehicle will approach from either directly behind or in front of the target.

The sensing system is expected to determine the bearing, range, yaw, pitch and roll and their rates from 100 feet to dock. Figure 1 shows the definitions of some basic terms. Our assumptions are that the vehicles have a reasonable GPS and ACS capable of bringing the vehicles into proper initial pose for the TRAC based sensor. It is further assumed that the ACS on the target vehicle is capable only of stabilizing the attitude pointing the target either ramward or wakeward. The chase vehicle however is assumed to be able to orient itself within 1 degree on command.

Nomenclature

Table 2 displays some basic nomenclature used throughout.

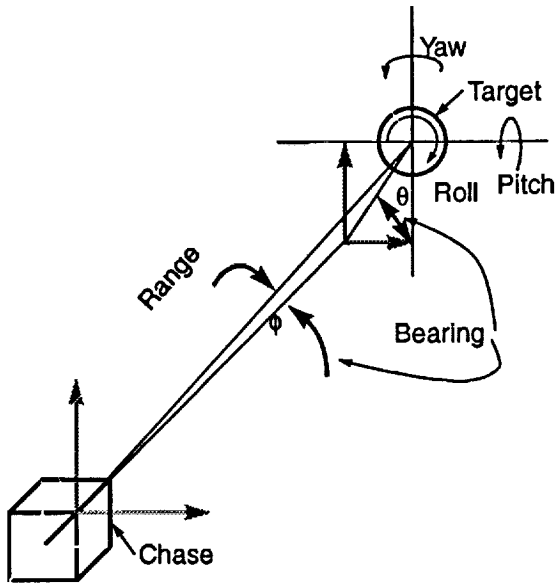

Figure 1: Definition of Errors.

Variable	Representation
Nearest Distance in Focus	$d_{\text{nearfocus}}$
Farthest Distance in Focus	d_{farfocus}
Distance Focused On	d_{focus}
View Angle	Θ
Focal Length	f
Distance to Image Plane	f_{image}
F Stop	F_{stop}
Pixel Size at Focus	x_f
Format Edge Length	l_{format}
Circle of Confusion	l_c
Range to Object	R_{ange}
Number of Pixel Rows	n_{pixel}
Diameter of Target	D_{target}
Sampling Period	D_{target}
Bearing	γ

Table 2: Nomenclature.

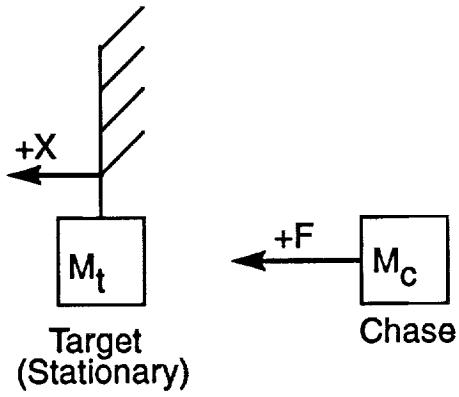

Figure 2: Definition of Variables for Range Analysis.

Sensor Requirements

This subsection presents a set of data indicating the required precision of the various errors. The data is used for comparison purposes only. The data is not official and should not be considered a statement of requirements.

Bearing Requirements The maximum bearing error used as a goal for this research is a constant $\pm 0.075°$. The bearing rate goal was specified as a constant $\pm 0.3°/s$. This data was obtained from conversations with colleagues who are experts in Shuttle rendezvous maneuvers.

Attitude Requirements The relative attitude requirements are functions of the docking probe used. It is believed that the relative attitude in yaw and pitch need to be $\pm 0.5°$, their rates need to be $\pm 2.0°/s$. Because of symmetry of the docking probe roll is not critical.

Range Requirements Data obtained from conversations with colleagues who are experts in Shuttle rendezvous maneuvers indicate that normally range precision must be better than one part in a thousand. This requirement is however biased in the sense that the specification assumes the range to several points is used to compute the attitude of the spacecraft. In our case, attitude is not obtained from the range data and therefore need not be as precise.

To obtain a realistic range and range rate requirement, a simple Phase Plane analysis was performed on the docking scenario. Figure 2 shows the definition of terms used in the following analysis. Our basic assumptions are that orbital dynamics are negligible (they certainly are for such a small maneuver), the target represents a Newtonian reference frame, both vehicles can be treated as point masses, the thrust (F) is bounded and there is no plume impingement.

A forbidden zone in the phase plane is defined as any point where if the chase vehicle enters it, it will surely crash into the target. The objective is to plot this

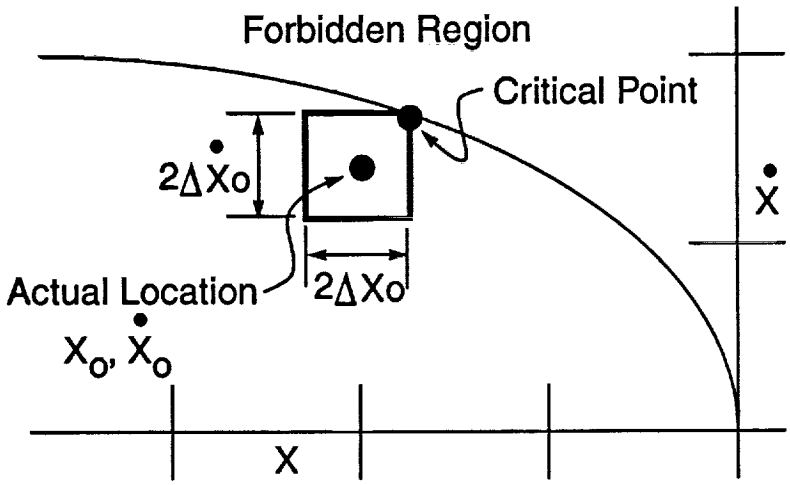

Figure 3: The Forbidden Zone, Showing the Chase Vehicle in an Acceptable Location.

forbidden zone. Clearly, any negative velocity of the chase is acceptable, provided it also has negative position (behind). For positive (closing) velocities, the edge of the forbidden zone is such that maximum thrust brings the chase to rest at the target. Hence, we let the thrust be maximum negative and initial chase position and velocity be $X_f < 0$ and $\dot{X}_f > 0$. Integrating the equation of motion for the chase and letting final position and velocity both be zero we obtain the equation for the boundary of the forbidden zone,

$$X_f = \frac{M_c \dot{X}_f^{\,2}}{2F}$$

which is plotted in figure 3. It is not difficult to recognize on which side of the boundary the forbidden zone lies.

Figure 3 also shows the chase vehicle in an acceptable region along with uncertainties in its range and range rate. What we seek is a relation between these errors and the state of the vehicle. Clearly, the worst condition is the upper right corner of the uncertainty bound because that is what would enter the forbidden zone first. If

$$X_o + \Delta X_o \leq \frac{M_c \left(\dot{X}_o + \Delta \dot{X}_o\right)^2}{2F} \tag{1}$$

then the vehicle is guaranteed to lie within the acceptable region. If velocity is computed from position as:

$$\dot{X} = \frac{X_{t+\delta} - X_t}{\delta}$$

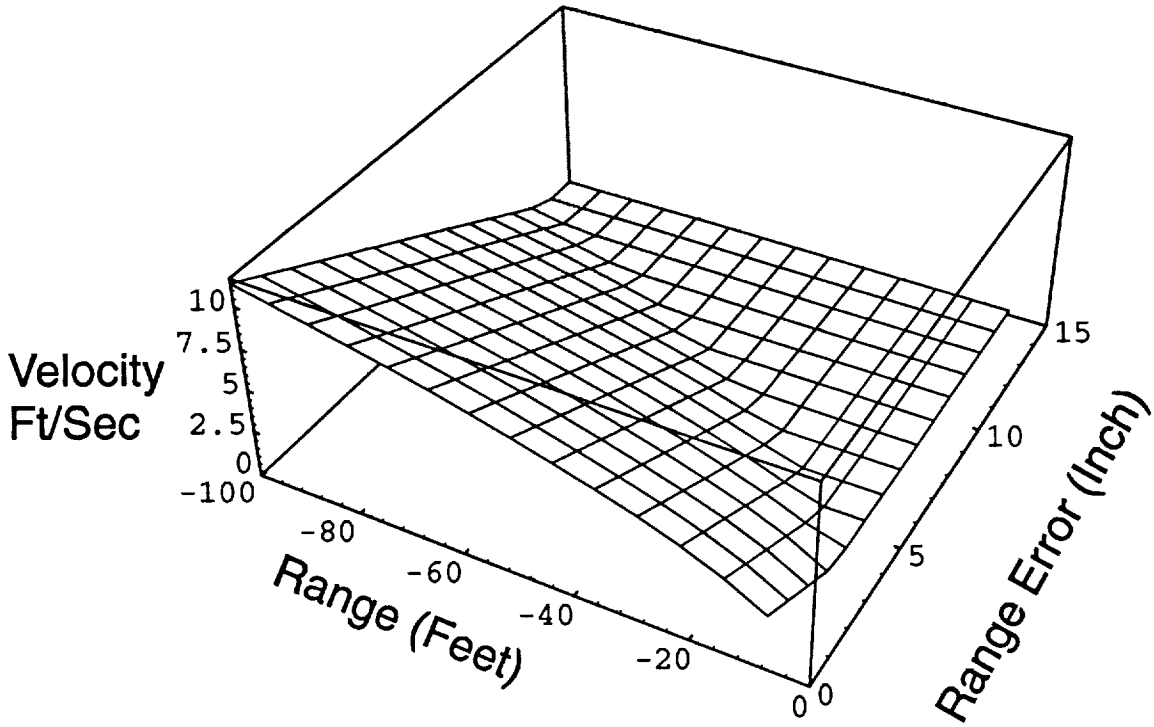

Figure 4: Maximum Velocity versus Range and Range Error for Large Ranges.

then the uncertainty bound (assuming zero error in time measurement) can be expressed (from equation 1) as:

$$\dot{X}_o \leq \sqrt{\frac{2F}{M_c}(X_o + \Delta X_o)} - \frac{\Delta X_o}{\delta} \geq 0 \tag{2}$$

Equation 2 demonstrates that one effect of measurement error is to limit the approach velocity. Using the parameters from Table 1 and $\delta = 0.1$s, one can solve for the maximum permissible approach velocity versus range and range error. This is shown in figure 4 for large ranges and figure 5 for smaller ranges.

An upper bound on the range error can be obtained by setting the approach velocity equal to zero and solving for the error versus range. This was done for the same parameter values and is shown in figure 6. It is not shown in the figures, but it is obvious that the error requirements relax as δ increases. Of course this analysis does not consider the effect of low sampling frequencies.

The Targeting Concept

The targeting concept has two distinct algorithms, one for short proximity operations and the other for docking operations. Essentially, we seek a sensing methodology

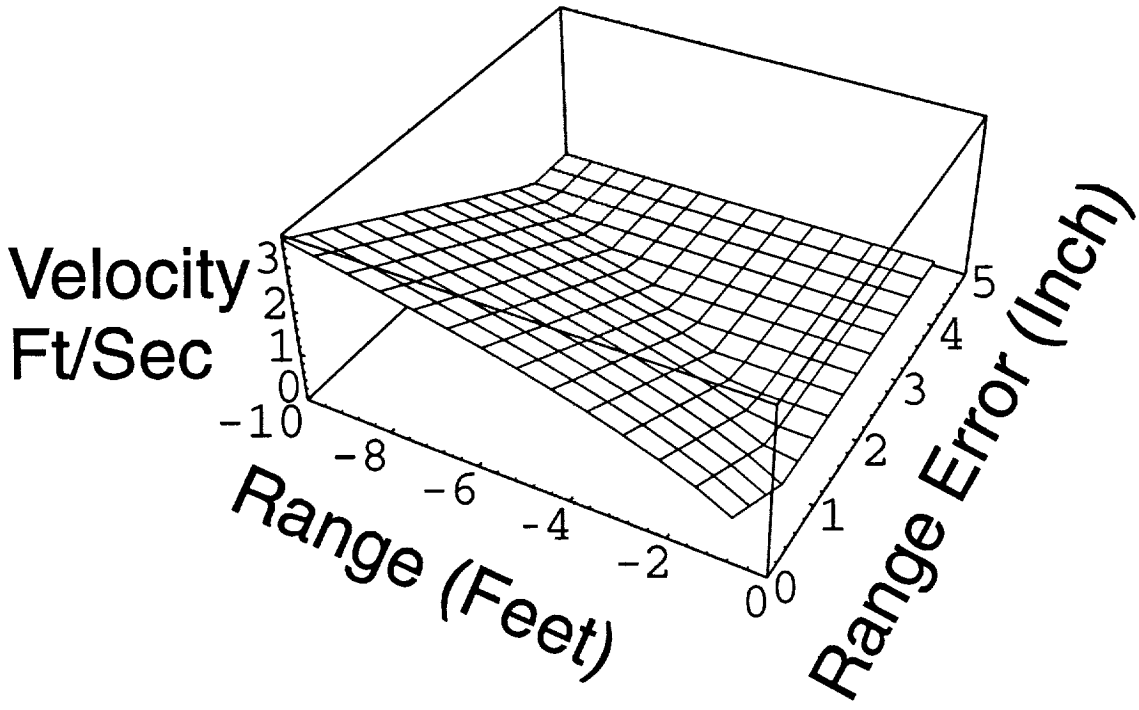

Figure 5: Maximum Velocity versus Range and Range Error for Small Ranges.

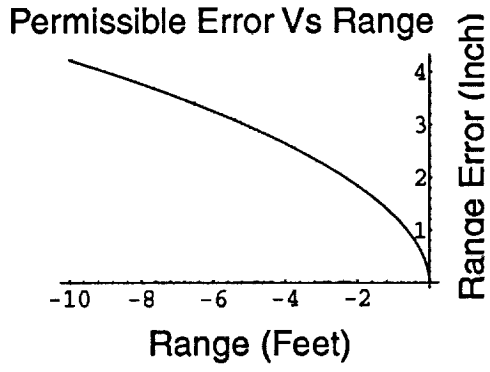

Figure 6: Permissible Range Error versus Range.

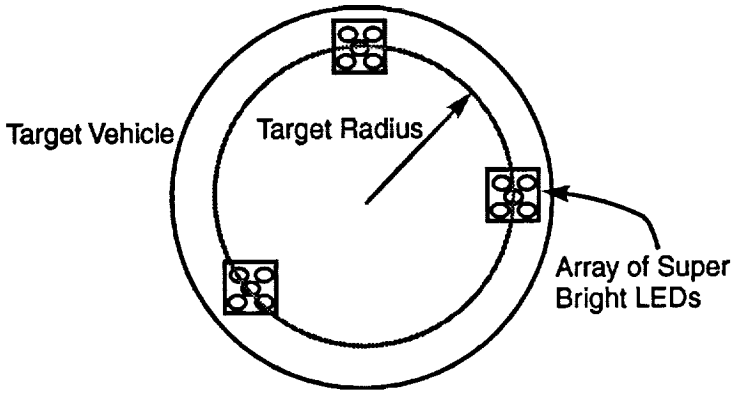

Figure 7: Active Beacon Target for Proximity Operations.

capable of handling long proximity and docking even though our experimental specifications only require 0 to 100 foot operations.

Proximity Operations In the general case, proximity operations occur at ranges as low as 1 foot and extend to thousands of feet. At such large distances, range and bearing information is the most critical. The most significant problem with visually sensing targets at such long range, is obtaining enough light energy on the sensor. In light of these two factors, we chose a beacon arrangement for proximity operations.

Figure 7 shows the target vehicle with three arrays of very bright LEDs mounted at a target radius. These beacons are flashed on and off at approximately the frame rate. The centroid of these beacons in the image allow the bearing to be computed. The perimeter formed by the beacons determine the range. The orientation of the target is determined by a perspective transformation using the three beacons. The ambiguity arising from using three rather than four points in the transformation does not concern us because we can resolve the ambiguity using information available from the ACS. Approximating the perspective transformation is simplified by the fact that orientation errors are small.

Docking Operations When the satellites reach some small range (chosen based on the sensor performance capabilities and requirements) the targeting concept switches to a conventional TRAC algorithm. The TRAC algorithm uses a flat mirror and three retroreflectors (bicycle reflectors) mounted on the target vehicle. The retroreflectors are mounted in a pattern similar to the beacons, except the target radius is smaller.

Lighting on the chase vehicle illuminates the flat mirror and the reflectors. The reflector image is used with an algorithm similar to the beacons to determine range, bearing, and roll. Figure 8 shows how this is accomplished. The image produced by the flat mirror is used to determine yaw and pitch. Figure 9 shows how this is done. The algorithm will not be explained here, the interested reader should consult [3].

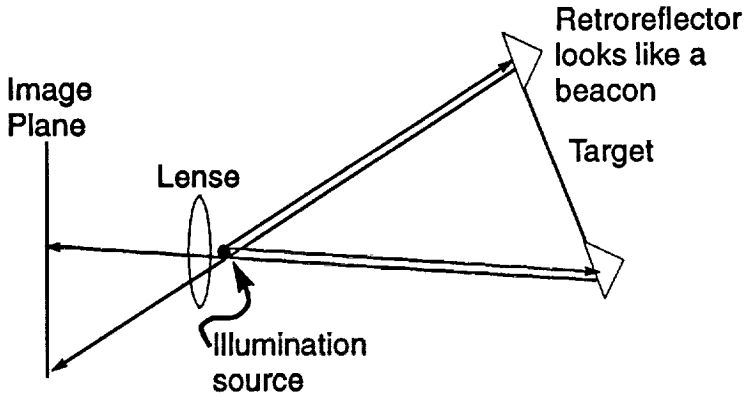

Figure 8: Using Retroreflectors with TRAC to Produce Beacons.

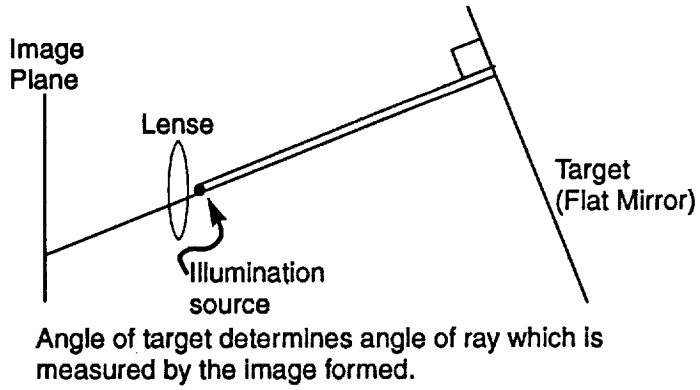

Figure 9: Using Retroreflectors with TRAC to Produce Beacons.

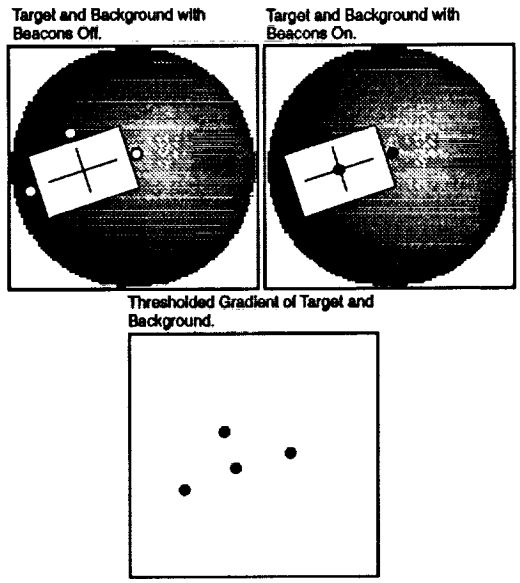

Figure 10: The Essence of the Filtering Technique Used.

Vision Robustness One very serious problem with any autonomous sensing system is robustness to extraneous sensations. In the case of a vision system, we need to be robust to background lighting, changes in illumination, occlusion and the like. Since our system has to be real time and inexpensive, we chose to use structured lighting as the solution to robustness.

We reduce the intensity of background lighting by using an interference optical filter which passes only the light wavelength emitted by our relatively single wavelength, blinking illumination source. Further noise rejection is obtained by time domain sampling the image to black out all pixels which do not blink at the rate of our source. Essentially, this is a filtering (or sampling) method. To reduce computational overhead, the lights are blinked to enable a filter arrangement to operate. Figure 10 shows a TRAC target illuminated by a source on the chase vehicle. The image contains a background, a flat mirror and three retroreflectors. Two images (for example) are taken in sequence and subtracted to determine the gradient of intensity for each pixel. Only the pixels that change produce bright spots in the image.

Of course, motion also produces a gradient and therefore one would expect some of the background to make it into the image. To reduce this effect, the second derivative (change of the gradient) is computed. Figure 11 shows how the algorithm will be implemented for the beacons, a similar procedure is used for the TRAC. Once the camera synchronizes with the beacons, we have images as shown in the first row. For simplicity the figure does not show background. Since we have control over the beacons, obtaining the images in the top row is possible. Next we subtract successive images to obtain images in the second row. Since this is simply a gradient, there will of course be some background due to changes in it. At this stage, pixel amplitude can

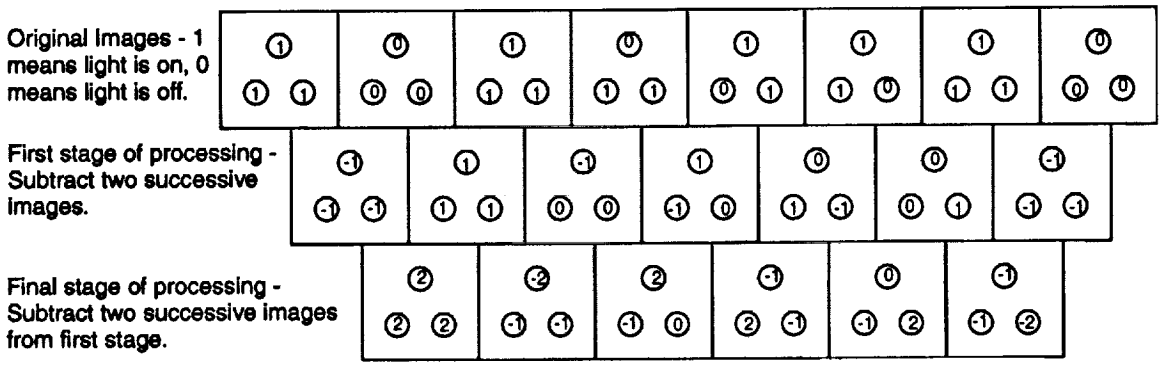

Figure 11: "Filter" Algorithm for Reducing Background Light Effects.

be positive, negative or zero. Most of the background will be close to zero. Images in the third row are determined by subtracting consecutive images in the second row. Essentially this is the second differential of the pixels. As you can see in the third row images, certain beacons have become accentuated because they illuminated at a certain time and then dimmed at an expected time. Now it is true that some background could become accentuated as well, provided it increases and decreases its brilliance at the correct time, however we feel the probability of that is small. After the second differential has been taken, we expect to threshold the pixels at a level determined by the maximum brilliance. What we expect to have in our image is either all, none or one beacon (we will know which). Therefore our vision processing can be a simple centroid calculation.

Video Equipment

This subsection presents a summary of the basic equations for choosing lenses, camera resolutions and the like. All of these equations are straightforward and can be found in most texts on photography. They are included only to assist those inexperienced in the area.

Lenses There are essentially two free parameters in a simple lense, the diameter and the focal length. The focal length (f) is the distance from the center of the lense to the point of focus of an object located infinitely in front of the lense. The Fstop (F_{stop}) is a dimensionless ratio of the focal length over the lense diameter. Once these parameters are specified, the lense is unique. In our calculations however there are several other quantities which make the calculations simpler.

Basic Vision System Specifications.

We established a set of basic specifications for our vision system which we then used to choose a lense system. These parameters are shown in Table 3. The minimum distance between the object and lense was specified by the design of the docking probe. The furthest distance we care to focus on was chosen arbitrarily. In actuality, all calculations were relatively insensitive to this parameter for distances greater than

Parameter	Value
Smallest Range to Focus on	1.22 Meter
Greatest Range to Focus on	1000 Meter
Desired Fstop Value	22
Diagonal Format Length	0.0127 Meter (.5 inch)
Number of Pixel Rows	512
Circle of Confusion	1 Pixel

Table 3: Basic Vision System Parameters.

100 feet. The desired Fstop value was chosen after experimenting with a camera and target system in bright daylight. The format length was chosen based on the fact that a typical half inch format has a good signal to noise ratio [4]. The number of pixels was selected arbitrarily. The circle of confusion is the radius of the circle (approximately) formed by "out of focus" light rays hitting the image plane.

Notice that we are specifying three quantities which define the lense system, the Fstop, the closest focused distance and the farthest focused distance. To satisfy these three specifications with our lense, we must select the focal length, Fstop and the point of focus to satisfy the near and far focus distances. To do this, we establish a relation between the specs and the distance to a sharply focused object as:

$$d_{\text{focus}} = \frac{2\, d_{\text{farfocus}}\, d_{\text{nearfocus}}}{d_{\text{farfocus}} + d_{\text{nearfocus}}}$$

and for the focal length we have:

$$f = \sqrt{\frac{2 l_c d_{\text{farfocus}} F_{\text{stop}} d_{\text{nearfocus}}}{d_{\text{farfocus}} - d_{\text{nearfocus}}}}$$

As expected, the focal length increases with the Fstop and decreases with the depth of field.

The view angle can be computed based on the focal length and the format length. Figure 12 shows the definition of the view angle. The angle shown is the angle when the lense is focused at infinity. It is computed as:

$$\Theta = 2\, \tan^{-1}\left(\frac{l_{\text{format}}}{\sqrt{\frac{8 l_c d_{\text{farfocus}} F_{\text{stop}} d_{\text{nearfocus}}}{d_{\text{farfocus}} - d_{\text{nearfocus}}}}}\right)$$

When focused at infinity, the image plane will be located at the focal length. When the lense is focused at the point of focus, the image plane will be located at:

$$f_{\text{image}} = \frac{d_{\text{nearfocus}} \sqrt{\frac{8 l_c F_{\text{stop}} d_{\text{farfocus}}^{\,3} d_{\text{nearfocus}}}{d_{\text{farfocus}} - d_{\text{nearfocus}}}}}{(d_{\text{farfocus}} + d_{\text{nearfocus}}) \left(-\sqrt{\frac{2 l_c d_{\text{farfocus}} F_{\text{stop}} d_{\text{nearfocus}}}{d_{\text{farfocus}} - d_{\text{nearfocus}}}} + \frac{2\, d_{\text{farfocus}}\, d_{\text{nearfocus}}}{d_{\text{farfocus}} + d_{\text{nearfocus}}}\right)}$$

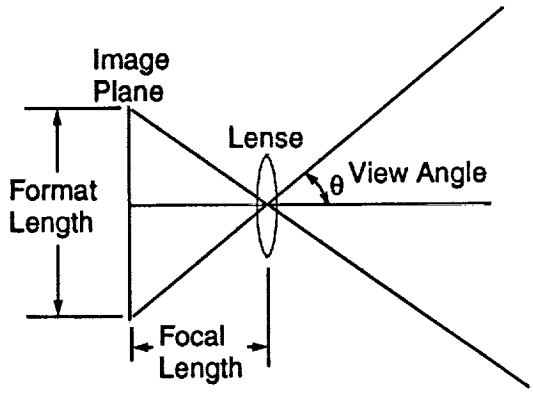

Figure 12: Definition of the View Angle.

Smallest Range in Focus	4 feet
Largest Range in Focus	1000 meter
Diagonal Camera Format	.5 inch
Number of Pixels per Side	512
Fstop	22
Length of Flat Mirror	1 foot
Target Diameter	2 feet

Table 4: System Specifications for the Example Calculations.

Targeting Performance

This subsection summarizes the performance of the targeting system. Table 4 gives the system specifications.

Rate Determination The rate of change of a signal is determined by differencing successive values. For example, if S_i is the signal at sample period i, then the derivative is approximately:

$$\dot{S}_i \approx \frac{S_i - S_{i-1}}{\delta}$$

Hence the error in the derivative calculation (due to measurement error) is a function of the signal error and the time error. We assume we have a very precise time measurement, therefore our derivative signal error is:

$$\Delta\dot{S} \approx \frac{2\Delta S}{\delta}$$

With the sampling time set to 0.1 seconds (three frames), the velocity error is 20 times the signal error.

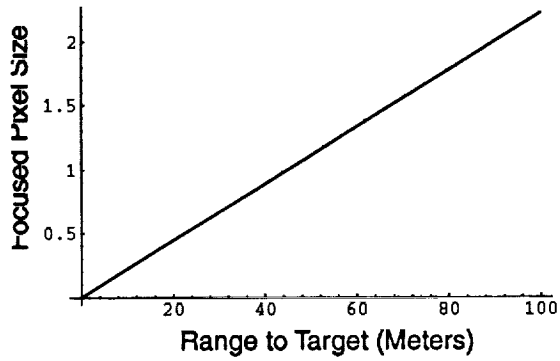

Figure 13: Focused Pixel Size versus Range.

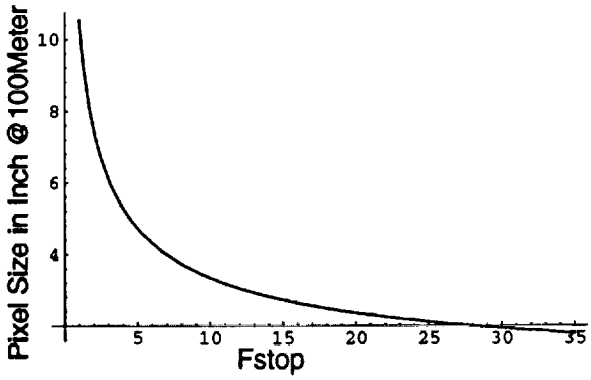

Figure 14: Pixel Size at 100 Meter Range versus Fstop.

Beacon Tracking When determining the position of an object, the camera measures position in pixels. A relationship can be determined which gives the actual size of a pixel. This relationship depends on where the image plane is and the range to the object. The pixel size when the image plane is focused at the point of focus is:

$$x_f = \frac{R_{ange} l_{\text{format}} \left(d_{\text{farfocus}} + d_{\text{nearfocus}}\right) \left(-\sqrt{\frac{2 l_c d_{\text{farfocus}} F_{\text{stop}} d_{\text{nearfocus}}}{d_{\text{farfocus}} - d_{\text{nearfocus}}}} + \frac{2 d_{\text{farfocus}} d_{\text{nearfocus}}}{d_{\text{farfocus}} + d_{\text{nearfocus}}}\right)}{\sqrt{\frac{8 l_c d_{\text{farfocus}}^3 F_{\text{stop}} d_{\text{nearfocus}}}{d_{\text{farfocus}} - d_{\text{nearfocus}}}} d_{\text{nearfocus}} n_{\text{pixel}}}$$

One pixel is what we assume is the smallest change in target position which can be measured. This of course assumes we cannot perform subpixel accuracy calculations. Figure 13 shows the relationship between the pixel size and range for the specifications given earlier. Figure 14 shows the relationship of pixel size to the Fstop. Figure 15 shows the relationship between the focus distance and pixel size is immaterial at distances above 50 meters. One concern is the maximum deviation from center which can be tolerated before one or more target beacons leaves the field of view. Figure 16 shows this value versus range. Of particular interest is the point when this becomes

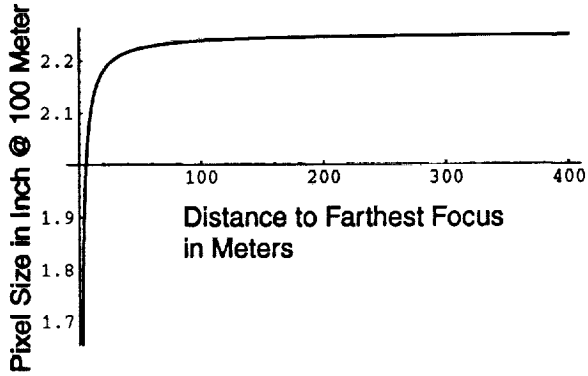

Figure 15: Pixel Size at 100 Meter Range versus Focus Distance for Fstop = 22.

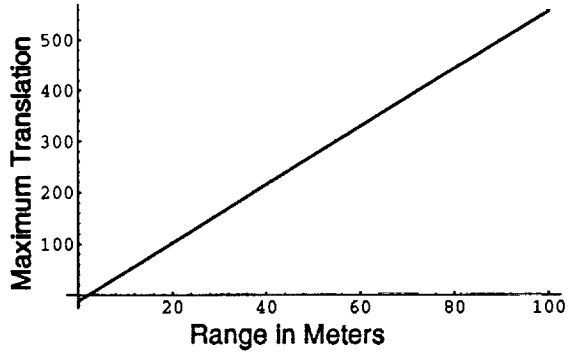

Figure 16: Maximum Translation Before Losing a Beacon.

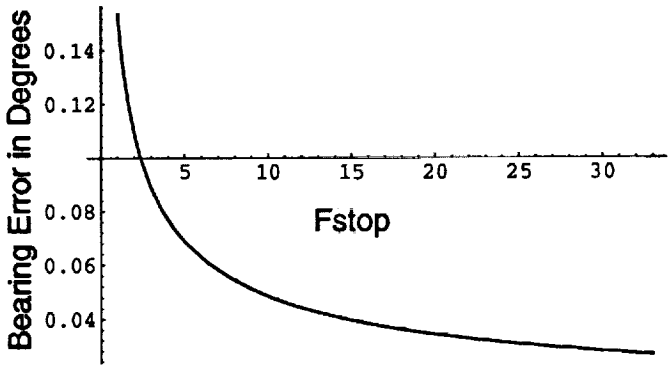

Figure 17: Bearing Error versus Fstop.

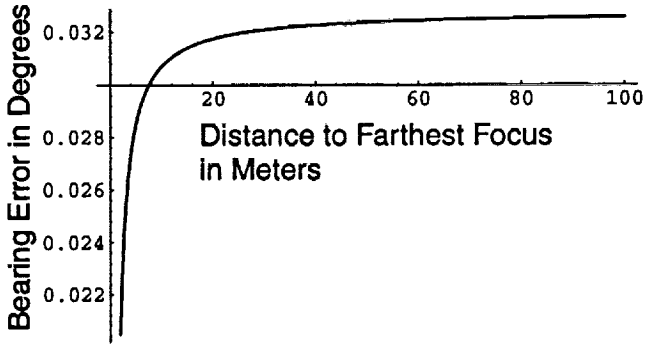

Figure 18: Bearing Error versus Focus Distance for Fstop = 22.

zero. At this point, it is impossible to keep all beacons in the field of view. For the specifications, this occurs at a range of 2.1101 meters.

These pixel sizes can be used to compute the bearing angle resolution as:

$$\gamma = \tan^{-1} \frac{p}{f}$$

The bearing angle, and hence its rate is constant with respect to the range. For the specifications, the bearing and its rate errors are 0.0327419° and $0.6\frac{\circ}{s}$. Comparing this to the required values of 0.07° and $0.3\frac{\circ}{s}$ demonstrates the system should satisfy the bearing requirements. Figure 17 shows the relation between bearing error and the Fstop. Figure 18 shows the effect of the focus distance on the bearing error.

Range is computed by comparing the separation distance between the beacons. Using such an algorithm means change in range can only be detected when the separation distance changes. We computed range error as the change in range required to produce a distinguishable change in separation. More specifically, we computed the change in range given a change in separation distance (a numerical derivative).

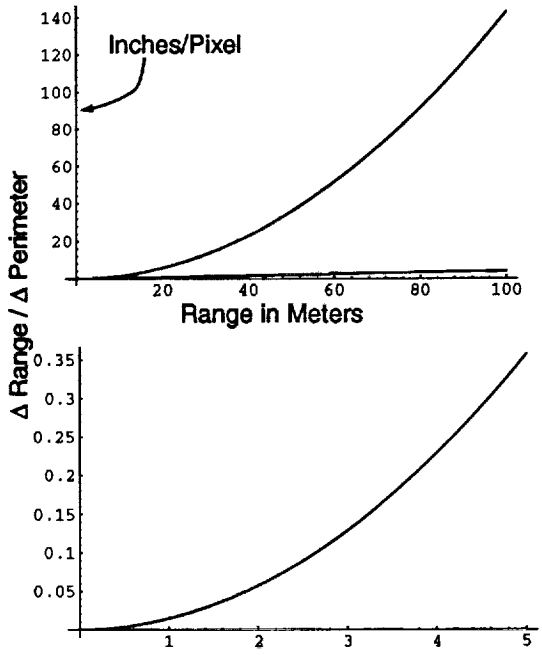

Figure 19: Range Error versus Range.

We assumed the target will be close to centered in the field of view. Based on the specifications, the change in range for a unit change in separation distance is shown in figure 19.

Attitude is determined using an inverse projection transformation. We computed the yaw and pitch attitude error as the smallest change in attitude that caused the separation distance between two beacons (at the same range) to appear to change. Figure 20 shows the smallest yaw and/or pitch required to produce a visible change in the image. The roll sensitivity is shown in figure 21.

When in close, the sensing algorithm switches from beacon following into a TRAC system. Determining the bearing, range and roll from the TRAC system is identical to that used in the beacons except the beacons are replaced with retroreflectors. Numerical differences in the errors occur because the "beacons" (retro reflectors) have a different configuration. Based on our specifications, figures 22 to 24 show the values for the TRAC system. Again the zero crossing (keeping all retros in the field of view) occurs at a range of 1.05505 meters.

Figure 9 demonstrates how TRAC determines the yaw and pitch of the target. It is clear from the diagram that it is equivalent to the calculation of a bearing angle, hence the resolution is independent of the range. For the specifications, the smallest angle measurable by TRAC is 0.0323314 degrees. The maximum angle measurable by TRAC depends predominately on the size of the mirror. Essentially, the reflected image "runs out" the mirror until it falls off the edge. The maximum measurable angle is shown in Figure 25.

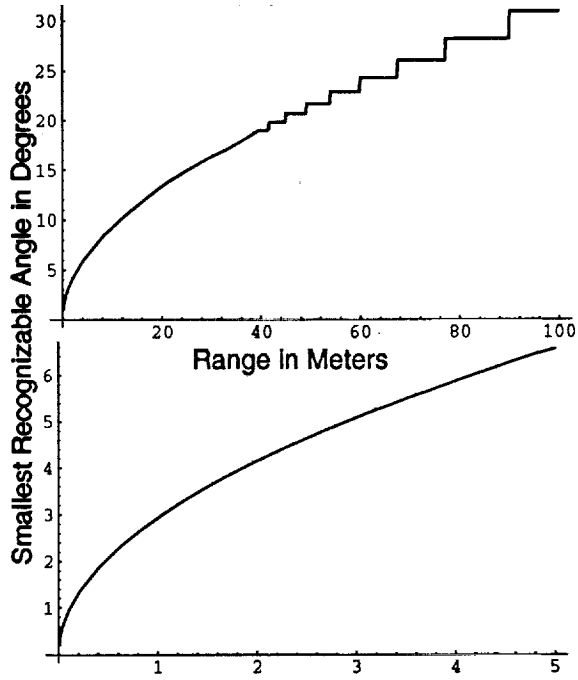

Figure 20: Smallest Recognizable Yaw (or Pitch) Angle Producing Noticeable Change in Image.

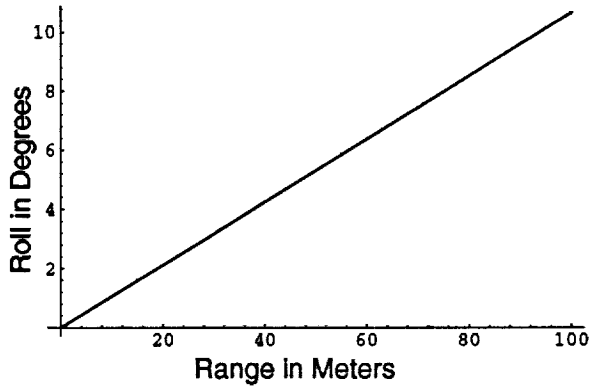

Figure 21: Smallest Recognizable Roll Angle.

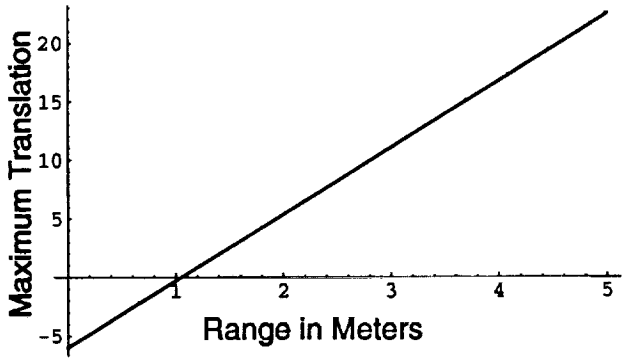

Figure 22: Maximum Translation Before Losing a Retro Reflector.

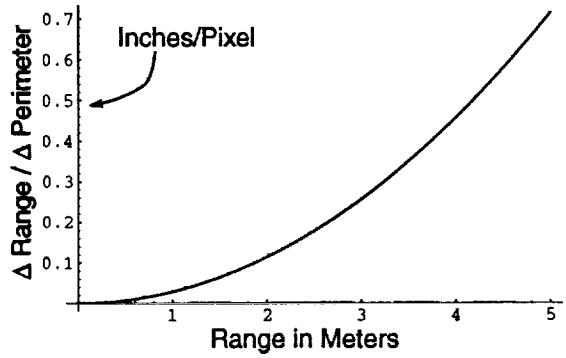

Figure 23: Range Error versus Range.

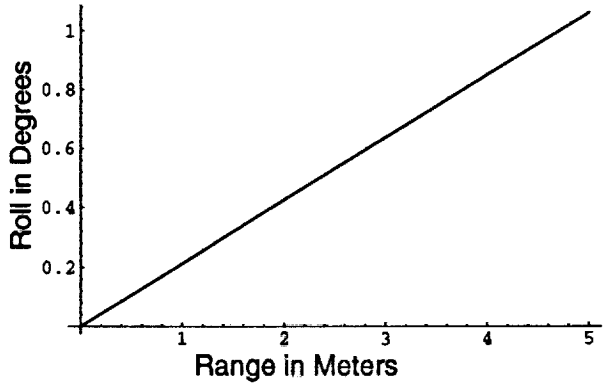

Figure 24: Smallest Recognizable Roll Angle.

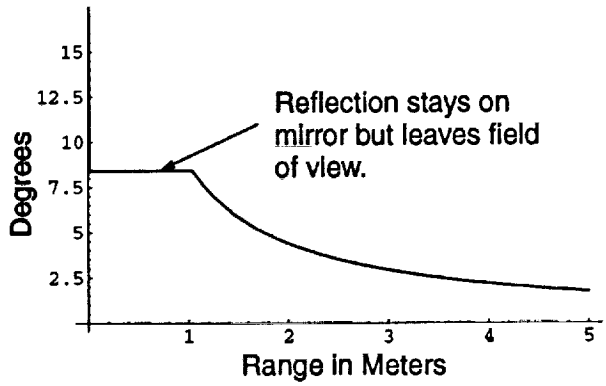

Figure 25: The Maximum Yaw and/or Pitch Angle Measurable by our TRAC.

Conclusions

This section presented a rendezvous and docking sensor system capable of performing autonomous rendezvous. The sensor is a simple single focal length, fixed iris CCD camera with structured lighting as the target. Analysis shows the system has sufficient resolution to enable the rendezvous. The chief limitation of the sensor is its restricted "field of view". This places constraints on the rendezvous trajectory, to enable the target to remain in the field of view. This restriction can be relaxed somewhat through the introduction of a variable lense system. When using the TRAC based portion of the sensor however, the maximum yaw and pitch deviation is set by the physical size of the target mirror. This may be relaxed by using a slightly curved mirror, but this is the subject of a forthcoming study.

LED LOADING

I was asked to investigate the proper method for connecting LEDs to a power source. This section documents this investigation. The LEDs used were "Kilobright" devices available from AND.

Based on the voltage current curve in the data book I determined the voltage drop for .2 amps to be 2.1 volts. This gives us a diode resistance of 10.5 ohms which I treat as constant.

Figure 26 shows three stages of leds. Each stage has 3 columns of diodes. This matrix was analyzed treating it as a resistor network. I used Mathematica to accomplish it. The input file is included in the next section.

Here are my results after some trial and error. I observed that if $R_s >> R_d$ then losing one resistor caused a serious overload on the diode. Likewise if $R_d >> R_s$ then losing one diode would overload a resistor hence I chose $R_d = R_s$. I also noticed that roughly 6.5 volts is needed to drive the network, hence a serious amount of power was wasted dropping down from 28 volts. Therefore I recommend conditioning the

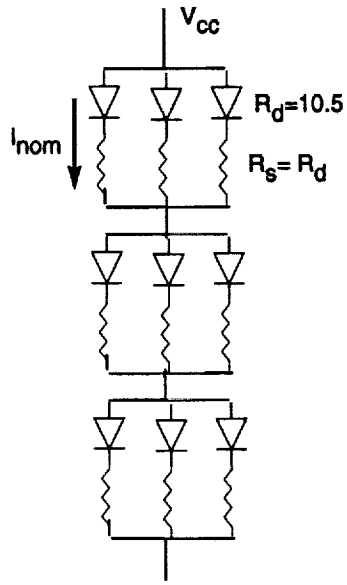

Figure 26: Nominal Led Matrix.

28 volts down to 6.5 in a more efficient manner than dropping it through a resistor.

With $V_{cc} = 6.5$, $R_s = R_d = 10.5$ the nominal current in each leg is 100 mA. The power dissipation is about 2 watts. If you short one resistor (or diode) in one leg, the maximum current in a leg becomes 168 mA. If two are lost on one stage and a third is lost on another stage, then the maximum current is 206 mA which is on the edge of smoking. If 3 legs open circuit, the current load is still within the 200 mA acceptable pulse current, however the power dissipation rises to about 3 watts.

Mathematica Input

This is the Mathematica input file.

```
numberofstages = 3
numberofelementsperstage = 3
dioderesistance = 21/2
seriesresistance = rs
globalresistor = ro
(*
rsgood = Table[1,{numberofstages},{numberofelementsperstage}]
diodegood = Table[1,{numberofstages},{numberofelementsperstage}]
*)
elementresistance = seriesresistance rsgood + dioderesistance
diodegood
invertedre = 1/elementresistance
units = Table[1,{numberofelementsperstage}]
unitsone = Table[1,{numberofstages}]
```

```
stageresistance = 1/ (invertedre.units)
totalresistance = stageresistance.unitsone + globalresistor
totalvolts = 6.5
totalcurrent = totalvolts/totalresistance
stagevoltage = totalcurrent stageresistance
elementvoltage =
Transpose[Table[stagevoltage,{numberofelementsperstage}]]
elementcurrent = elementvoltage / elementresistance
nominalelementcurrent = 100/1000
nominalrs =
Solve[(nominalelementcurrent==elementcurrent[[1,1]])/.ro->0,rs]
nominalro =
Solve[(nominalelementcurrent==elementcurrent[[1,1]])/.rs->diodere
sistance,ro]
```

SUPPORT OF THE EXPLORER PLATFORM

The explorer platform is a space craft, to be launched from the Shuttle, and will perform scientific experiments. After the experimentation, it will be retrieved using some type of rendezvous device. It is therefore an excellent opportunity to test targets. As a result, Leo Monford began the development of all metal retroreflectors which could be mounted on the Explorer. I was asked to make quick reflectance tests of these reflectors. What we were interested in was the usefulness of the reflectors for cameras. A series of tests on the reflectance versus wavelength was performed under a separate study and will not be documented here.

Test Results

On December 28, 1991 I tested seven types of reflectors. 1. An aluminum retro made by John Casstevens, 2. A white plastic reflector made by Stimsonite, 3. A red plastic reflector (manufacturer unknown), 4. The same red reflector with the cardboard backing removed, 5. The red reflector without its backing and placed backwards, 6. The Stimsonite reflector without its white plastic backing, and 7. A metal reflector sheeting produced by Vacuum Process Engineering.

I placed the reflectors 36 feet from a camera and shot a laser at them. I placed a paper "screen" behind the laser to view the appearance of the reflection. All reflectors had grainy, yet distinct bright spots coming from each cell of the reflector. They all had approximately the same spreading.

The camera's Fstop was set to its maximum (22). I captured an image with all lighting off and determined the brightness of the background. The background illumination ranged from 48 to 53 (255 is brightest white).

The laser, reflector and camera were set up as shown in figure 27.

For each measurement, I captured an image, placed a rectangle around the reflected light blob and performed statistics on the information inside the rectangle. The rectangle dimensions were:

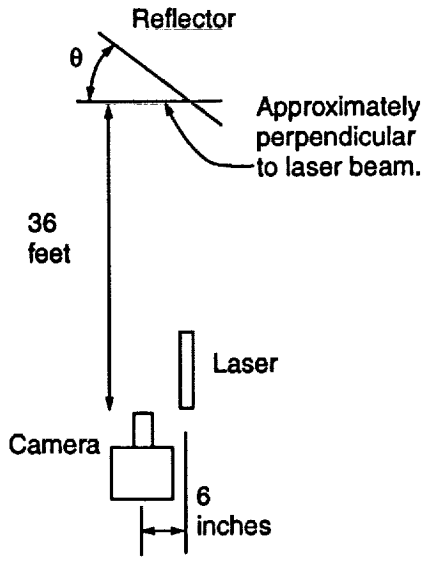

Figure 27: The Experimental Setup.

Number of Pixels	169
X dimension	13 pixels
Y dimension	13 pixels

In the following data, the values are for the information inside the rectangle.
For John Cassteven's reflector, the following was obtained.

Angle θ	% of Pixels > 100	# at Brightest	Brightest	Average	Variance
0	26	23	255	105	5906
15	17	1	255	82	4086
30	4	1	244	54	681

For the white Stimsonite reflector, the following was obtained.

Angle θ	% of Pixels > 100	# at Brightest	Brightest	Average	Variance
0	31	35	255	110	6322
15	25	22	255	97	5516
30	14	13	255	75	3353

For Red reflector with its backing, the following was obtained.

Angle θ	% of Pixels > 100	# at Brightest	Brightest	Average	Variance
0	62	63	255	163	6770
15	37	40	255	121	6630
30	21	21	255	90	4797

For Red reflector (front surface) without its backing, the following was obtained. I observed that significant light passed through the reflector.

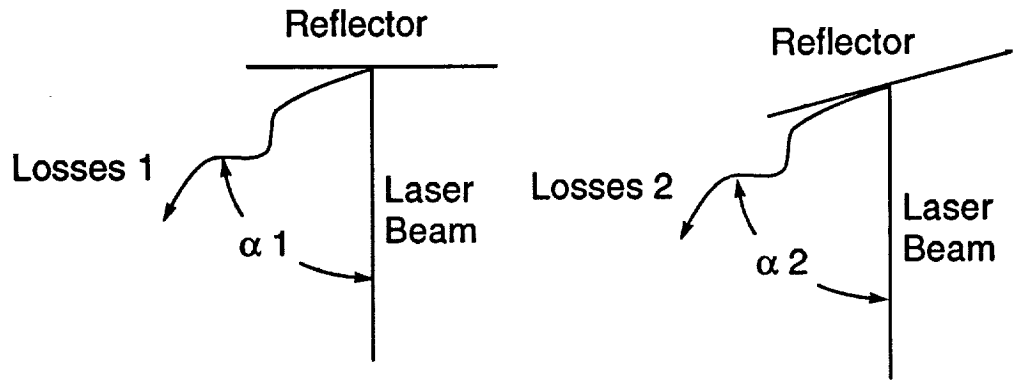

Figure 28: Observed Losses From Reflector.

Angle θ	% of Pixels > 100	# at Brightest	Brightest	Average	Variance
0	56	60	255	152	7270
15	20	16	255	85	4222
30	21	8	255	68	2536

For Red reflector (back surface) without its backing, the following was obtained. I observed that most of the incident light passed through the reflector.

Angle θ	% of Pixels > 100	# at Brightest	Brightest	Average	Variance
0	0	1	84	49	21
15	0	13	48	48	1

For White Stimsonite reflector no backing, the following was obtained.

Angle θ	% of Pixels > 100	# at Brightest	Brightest	Average	Variance
0	94	116	255	218	3776
15	23	19	255	92	4751
30	7	5	255	63	1758

For metal vacuum formed reflector, the following was obtained.

Angle θ	% of Pixels > 100	# at Brightest	Brightest	Average	Variance
0	33	35	255	sorry	sorry
15	56	57	255	sorry	sorry
30	32	32	255	sorry	sorry
70	9	6	255	sorry	sorry
60	35	35	255	sorry	sorry
0	25	26	255	sorry	sorry

In addition to the data, I observed the following regarding John's reflector. When the laser hit the reflector, there were significant "losses" from the reflector. What I mean by this is that there were very bright rays reflecting from the reflector in directions other than the incident direction. Figure 28 shows what I mean.

I observed that these losses came off in three basic directions (actually there was a

cone of light but I found it to be very intense in only three directions). I also observed the following relations: losses 2 >> losses 1 and $\alpha_2 << \alpha_1$.

EXAMPLE PERFORMANCE

This section gives performance results for a camera placed 50 feet from a TRAC target. It assumes the following values:

Parameter	Value
lengthofflatmirror	1 foot
nearrequired	4 foot
farrequired	1000 meter
fstopdesired	16
formatlength	1/2 inch
numberofpixelrows	512
circleofconfusion	1 pixel

Here are some numerical values at 50 foot distance for two target sizes.

Parameter	Value 1	Value 2
Target Diameter in inches	24	12
fstop	16.	same
focallength in millimeter	31.1	same
smallest yaw change recognizable in degrees (using beacons)	13.7	19.8
smallest roll angle measureable degrees	2.25	4.51
Maximum flat mirror trac capture angle plus minus degrees	0.573	same
Smallest measurable flat mirror angle degrees	0.0451	same
Pixel Size inches	0.472	same
allowed translation error inches	109.	115
allowed rotation degrees plus or minus	10.5	11
Smallest change in range in inches	4.62	9.24
perimeter size in pixels	129.	62.7

Figures 29 through 36 assume a 24 inch target diameter.

AUTONOMOUS GRAPPLING OF AN H HANDLE

The objective of this assignment was to implement the Auto TRAC on a PUMA 700 series robot and use it to grapple a handle. The target mirror was approximately 3 inches square.

One operation of the autotrac is a find algorithm which attempts to orient the camera normal to the mirror with sufficient accuracy to cause the camera's mirror

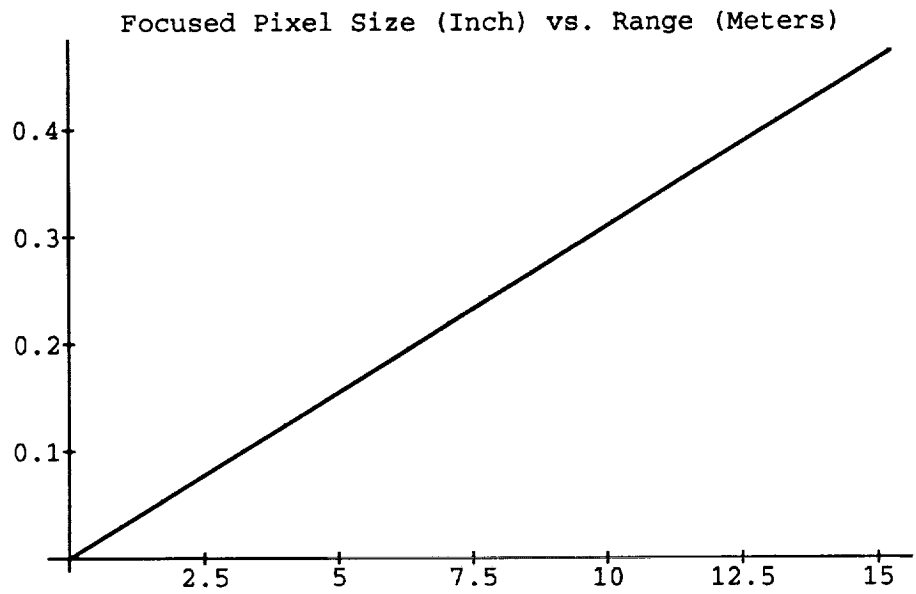

Figure 29:

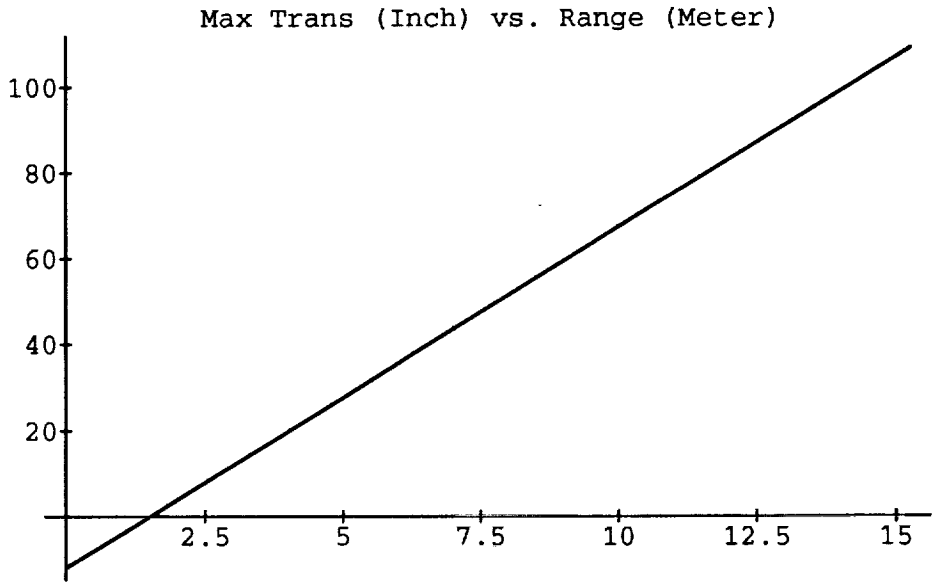

Figure 30:

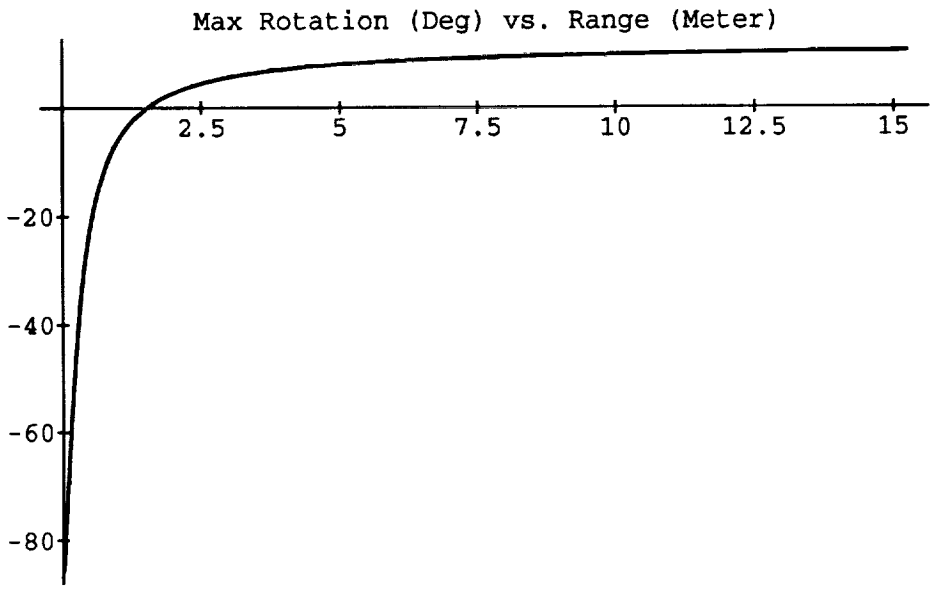

Figure 31:

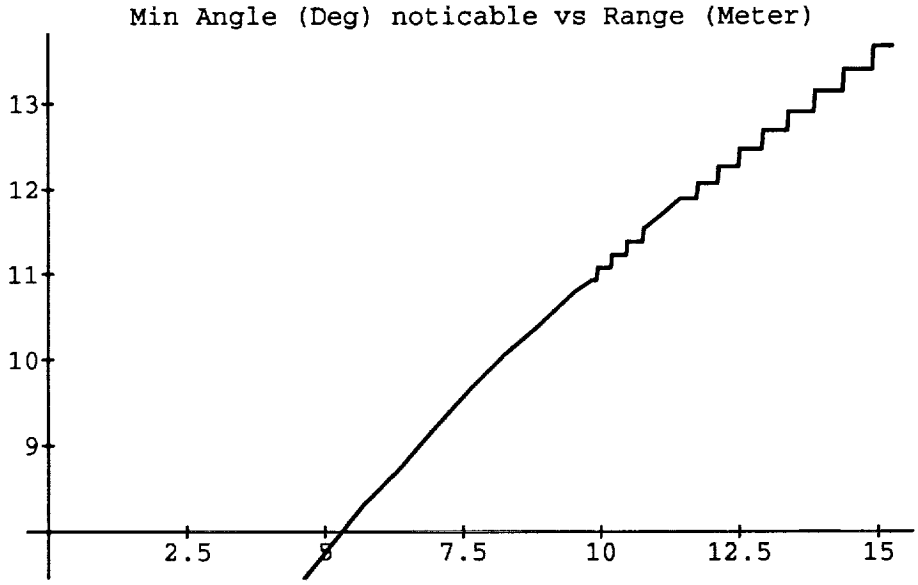

Figure 32:

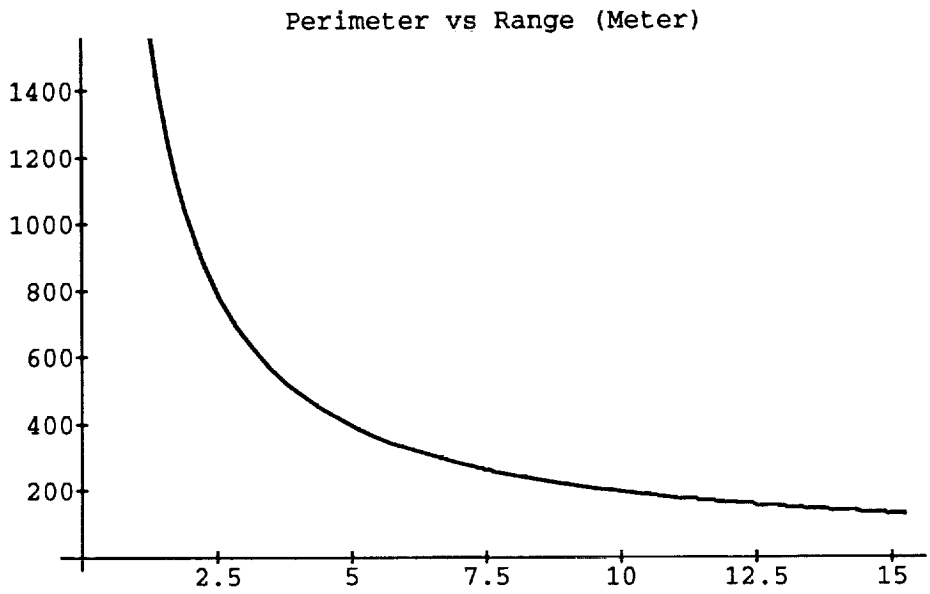

Figure 33:

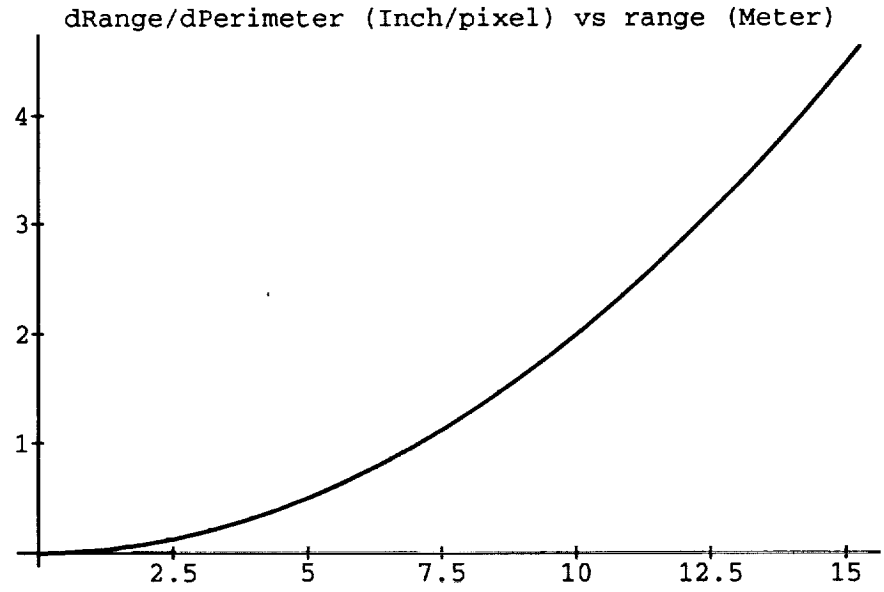

Figure 34:

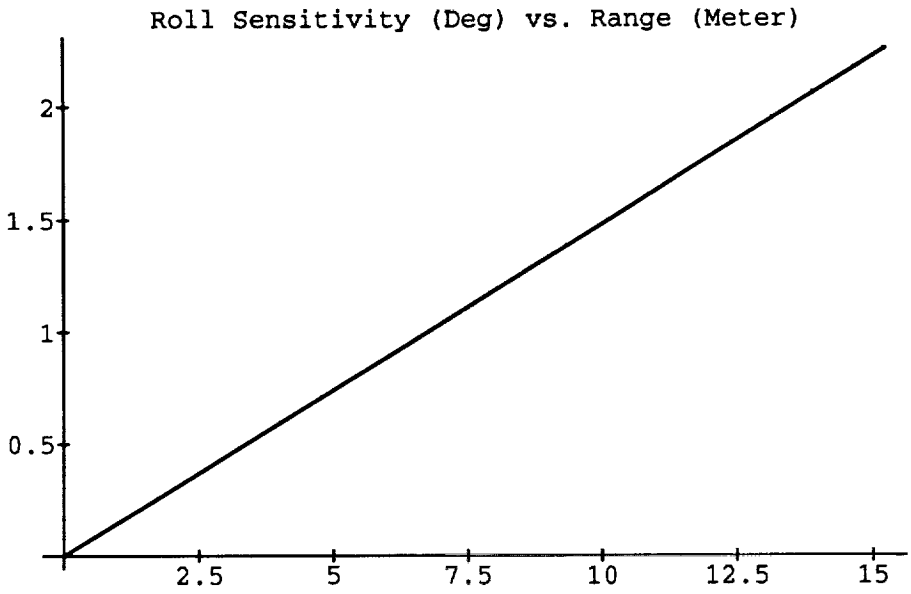

Figure 35:

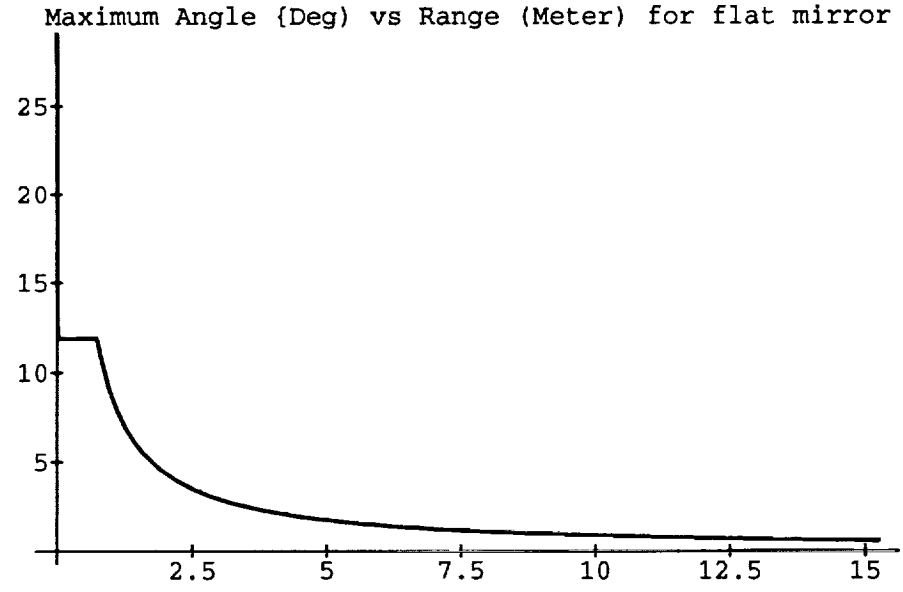

Figure 36:

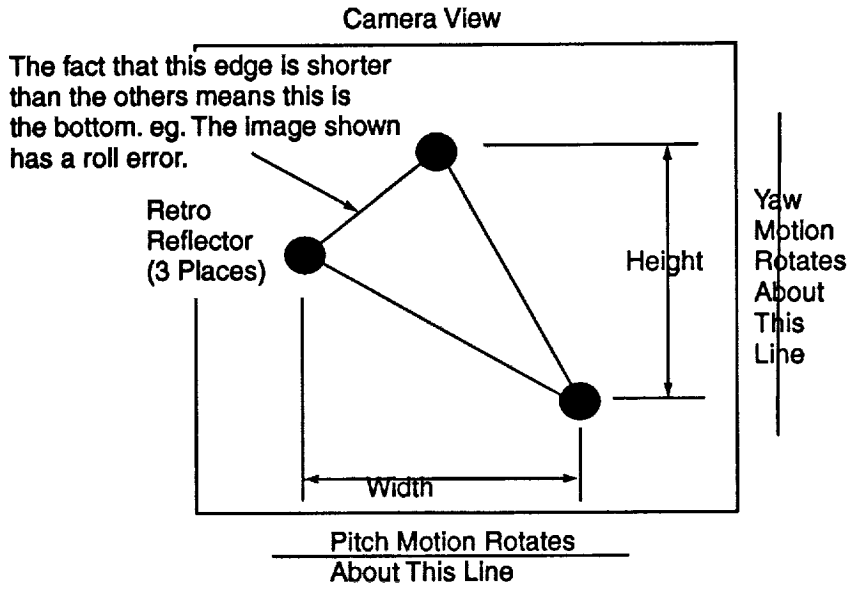

Figure 37: Definitions Used in the New Find Algorithm.

reflection to become visible by the camera. The previous algorithm compared the triangular perimeter formed by the three retro reflections at two vantage points. The robot was moved in the direction which maximized the perimeter. The idea was that the perimeter formed by the three retros would be largest when the camera is normal to the mirror. Of course this requires the range to remain constant at the two vantage points. The algorithm worked reliably when using a large mirror and wide angle camera lense.

When using a small target size and relatively narrow camera field of view, the original find algorithm did not work reliably. Therefore a new algorithm was required. The basic problem was that as the robot rotated about the mirror, it changed its range by small amounts. This was due to the fact that the robot could not be made to rotate exactly about the mirror. Therefore what we needed was an algorithm which worked independent of range.

The new algorithm takes a ratio of retro triangle width to height. Figure 37 shows the configuration for the new find algorithm. If the robot is attempting to correct the yaw then the robot moves to maximize the width/height. To correct the pitch, it maximizes the height/width. The new algorithm was tested on the system and performs reliably.

THE PERFORMANCE WHEN USING A POST ON THE TARGET.

This project was to estimate the performance of the sensor when a post protrudes from the target. The calculations were performed using Mathematica and the results are shown in the Mathematica notebook form included in Appendix A.

PSD - Position Sensitive Device.

The PSD device was conceived at the New Initiatives Office and implementation was begun in March. The PSD device should be under consideration for patent protection and as such it cannot be documented in this report.

Fourier Analysis

When discussing the operation of the PSD, the question of how multiple frequencies could be extracted from a single signal was raised. One method of doing this of course is to use Fourier Analysis. An example problem of using FA is included as Mathematica output in Appendix B.

EVALUATION OF A CURVED MIRROR FOR TRAC

Leo Monford asked for an evaluation of a curved (spherical) mirror for potential use on a TRAC sensor. The advantage is that the maximum measurable pitch/yaw angle increases significantly from what is possible with a flat mirror. It was determined that a negative effect of curvature is to cause the reflected image to appear further away than it really is. For example, the reflected images appear smaller than normal. This reduction in size is accompanied by a decrease in the amount of light reaching the sensor. Because there is concern about being able to achieve the required light intensity at large range, the effective range with a curved mirror was determined. The maximum pitch and yaw angles which can be sensed using a curved mirror is approximately equal to the solid angle formed by the mirror, hence smaller radii mirrors offer the most improvement.

Figure 38 shows the setup for the analysis. The circle represents the curved mirror with radius r. The observer is located d to the right. A light ray travelling at an angle B from normal to the mirror (horizontal), strikes the mirror and moves away with the angle $2T + B$ from horizontal. Eventually the ray travels a horizontal distance d at which point the light ray has travelled vertically X. Note that if r, B, and d are known, X can be computed.

Now for a flat mirror, the same ray would travel with an angle of B from horizontal after reflecting. As a result, when it returns a horizontal distance d, it has moved a smaller vertical distance (call it h).

What all of this means is that a ray which emanates from X and hits the curved mirror "looks" like a ray which emanates from h and hits a flat mirror. Hence a large object appears smaller.

What we are interested in however is the effective range of the light ray striking the curved mirror. To determine this we compute what horizontal distance a light ray would have to travel so that it travels a vertical distance of X after striking a flat mirror.

These calculations were computed using a Mathematica script and the results are given in figure 39. Notice that as the mirror radius decreases (good for the maximum

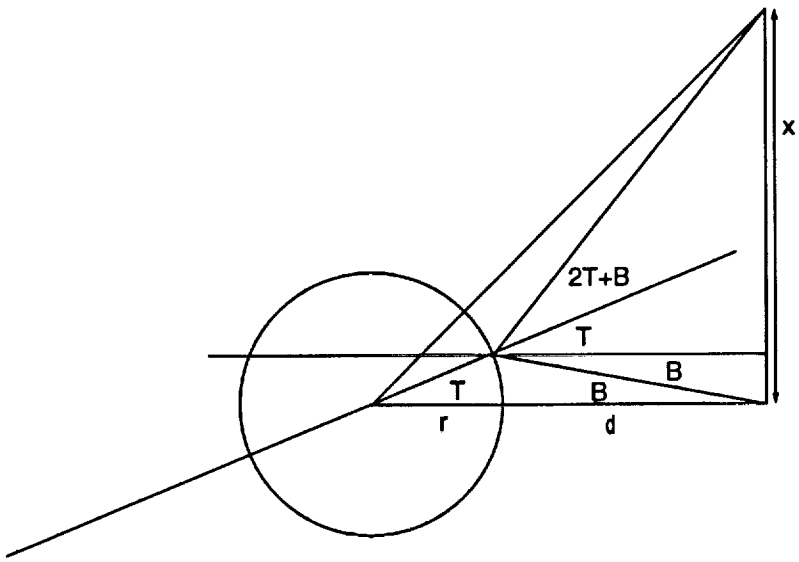

Figure 38: Problem Formulation for the Curved Mirror.

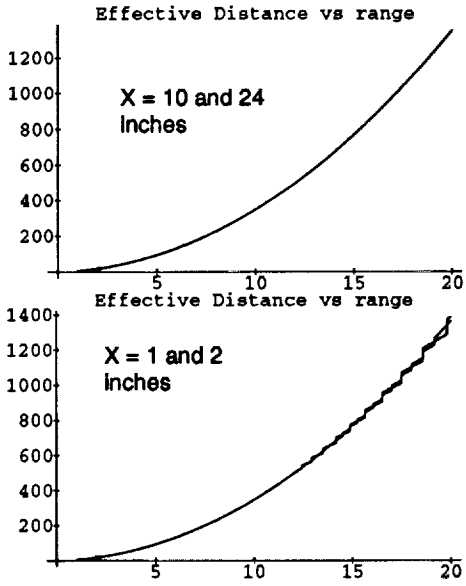

Range is distance to mirror / radius of mirror. Effective distance is distance / radius of mirror.

For a 24 inch radius mirror, 20 corresponds to 12.192 Meter and 1400 is 853.44 Meter

Figure 39: Effective Distances for Selected Values of X.

angle measurements) the effective distance increases (bad for the illumination). The conclusion is that curved mirrors are probably not a valid option.

REFERENCES

[1] P. T. Jr., M. E. Dobbs, D. J. A. Jr., D. J. Conrad, M. P. Frazer, and D. K. Slayton, "Autonomous rendezvous and docking using an expendable launch vehicle," in *Utah State University conference on Small Satellites*, AIAA, August 1991.

[2] L. Monford, "Docking alignment system," U. S. Patent No. 4890918, NASA JSC Case No. MSC 21372-1.

[3] R. Redfield, L. J. Everett, M. Bradham, and J. Pafford, "Autonomous TRAC," Final Report for NASA Grant NAG3-96, Texas A&M University, Mechanical Engineering Department, College Station, TX 77843-3123, December 1991.

[4] *Solid-State Imaging Devices, Tech Note No. T1007.* Vicon Industries Inc., 525 Broad Hollow Road, Melville, Ny 11747-3703, August 1988.

THIS IS THE RESOLUTION OF YAW AND PITCH WHEN USING A POST

This routine is to calculate the minimum angle you can measure if you use a post on the target.

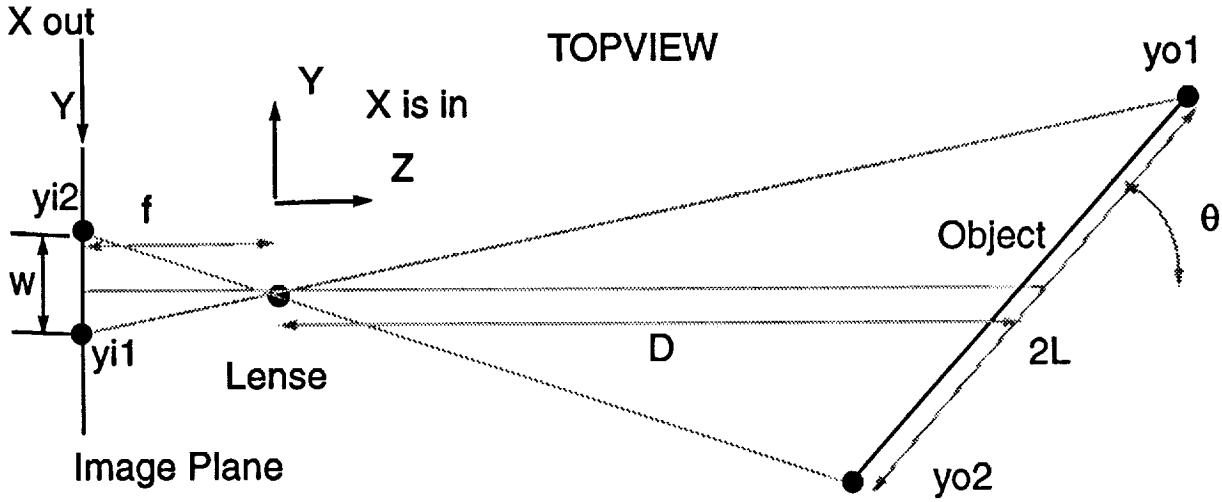

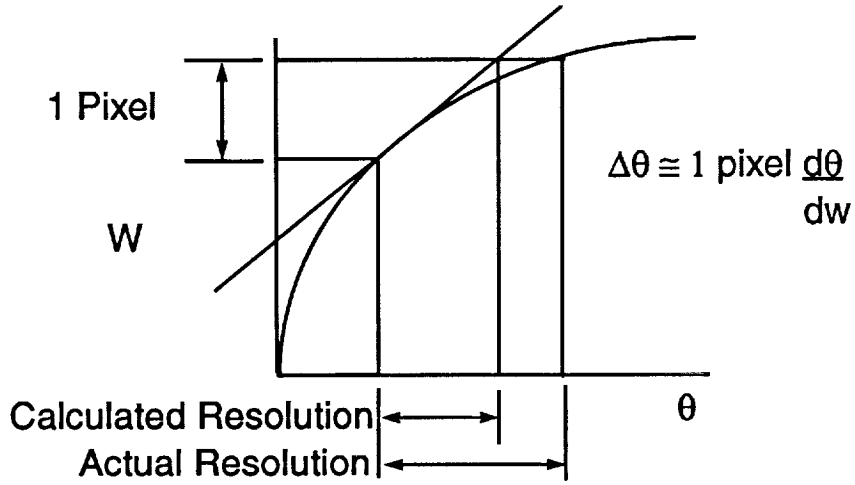

Include unit calculations.

```
<<$Math/units.h;
```

We calculate the y coordinates assuming the length L and θ are given. Note that θ is a number in radians.

```
yo1 = L Sin[θ];
yo2 = -L Sin[θ];
```

Next are the perspective transformation equations. Similar triangles which relate y on image plane to y of object. Note that θ is a number in radians.

```
eq1=yo1/(D+L Cos[θ]) == yi1/f;
eq2=yo2/(D-L Cos[θ]) == yi2/f;
```

Next we solve these equations for the image plane positions. These are y1 and y2.

```
ans = Solve[{eq1,eq2},{yi1,yi2}];
y1 = ans[[1,1,2]];
y2 = ans[[1,2,2]];
```

Calculate w as a function of θ, it produces an equation for w containing D and L. Note that ct must be a number in radians.

```
w[ct_] := (y1-y2)/.θ->ct;
Plot[(w[zz Degree]/Meter/.{D->10 Meter,L->12 inch,f->19 millimeter}//
Plot[1/(w'[zz Degree]/Meter/.{D->10 Meter,L->12 inch,f->19 millimeter
```

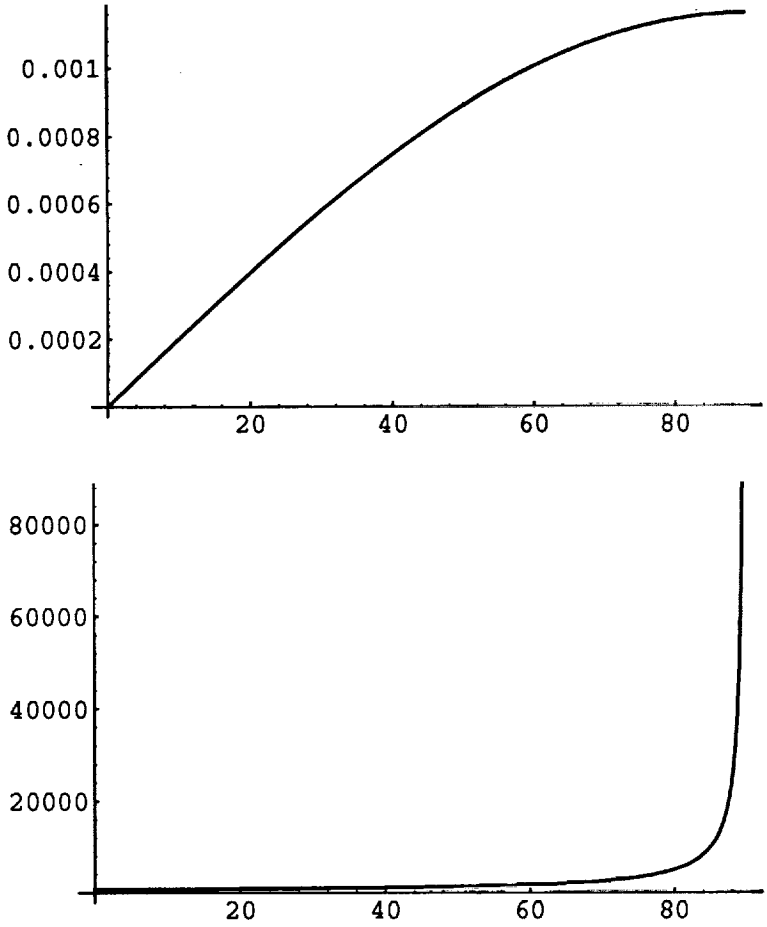

-Graphics-

The above graphic shows a typical w versus θ. and a typical 1/w' versus θ

dang[θ] calculates 1 pixel / (derivative of w with respect to θ). It is Δθ shown in the figure above. The argument must be a number in radians. It produces an angle in radians also.

```
dang[tt_]:=(pixel/w'[tt]);
```

The above calcualation is not even close when q is near 90 so we can also use a bisection.

```
<<$Math/bisect.h;
bisecteqn[tt_]:=pixel-Abs[w[tt]-w[tt+resolution]];
```

dp[min,max,D,L] plots Dq versus q from min<q<max min and max assumed to be numbers in degrees

```
dp[min_,max_]:=Plot[dang[x Degree] /.{Meter->1},{x,min,max}];
```

Now for some constants

```
f=19 millimeter;
formatlength=Sqrt[(1/2)^2/2] inch;
numberofpixelrows=512;
pixel=formatlength/numberofpixelrows;
```

Next we define the post height h and the separation s. See the following figure.

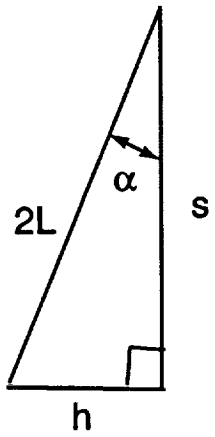

Here s is the distance along the target, h is the elevation of the post. α and L are calculated as

```
α=ArcTan[h/s];
el=Sqrt[h^2+s^2]/2;
```

If the flat target is located at some θ=θf, then the post target θ=θp is θp=θf-α.
diff takes an angle in degrees and returns the difference in sensitivity also in degrees.

```
θf=θ
θp=θf-α
flattarget:=dang[θf]/.L->s/2
bisectflat:=bisecteqn[θf]/.L->s/2
posttarget:=dang[θp]/.L->el
bisectpost:=bisecteqn[θp]/.L->el
diff[dd_]:=((flattarget-posttarget)/.θ->(dd Degree))/Degree
plotdiff[min_,max_,range_]:=Plot[diff[x]/.D->(range),{x,min,max}]
```

Now define post height and separation distance.

```
h=2 inch;
s=12 inch;
```

The following finds the difference in resolution between the post and flat targets.

```
bisectdiff[dd_,range_]:=Abs[
    Bisect[0,90 Degree,.00001,
        (((bisectflat/.q->(dd))
        /.D->(range))/.Meter->1),resolution]-
    Bisect[0,90 Degree,.001,
        ((((bisectpost)/.q->(dd)))/.D->(range))/.Meter->1,resolution]
        ]/Degree//N

bisectdiff[90 Degree,10 Meter]

12.2707
```

From the above the post is 12 degrees better than is the flat target. This is when the target is perpendicular to the optical axis (worst case is some sense).

```
bisectdiff[90 Degree,.1 Meter]

0.694542
```

When the range is .1 meter there is only .7 degrees difference between the post and flat.

```
Bisect[0,90 Degree,.00001,
        (((bisectflat/.q->(90 Degree))
        /.D->(10 Meter))/.Meter->1),resolution]/Degree//N

14.1404
```

The above shows that the flat target at 10 meters provides (worst case) + - 14 degrees yaw and pitch resolution. In what follows we repeat for the other dimension.

```
h=2 inch;
s=30 inch;

bisectdiff[dd_,range_]:=Abs[
    Bisect[0,90 Degree,.00001,
        (((bisectflat/.q->(dd))
        /.D->(range))/.Meter->1),resolution]-
    Bisect[0,90 Degree,.001,
        ((((bisectpost)/.q->(dd)))/.D->(range))/.Meter->1,resolution]
        ]/Degree//N

bisectdiff[90 Degree,10 Meter]

4.55074
```

Here the flat is only 4.5 degrees worse than post when at 10 meters

```
bisectdiff[90 Degree,.1 Meter]

0.124626
```

Here the flat is only .1 degrees worse than post when at .1 meter range.

```
Bisect[0,90 Degree,.00001,
        (((bisectflat/.q->(90 Degree))
        /.D->(10 Meter))/.Meter->1),resolution]/Degree//N

8.94047
```

the flat target provides 8.9 degree resolution at 10 meters range.

```
plotdiff[90,45,10 Meter]//N
```

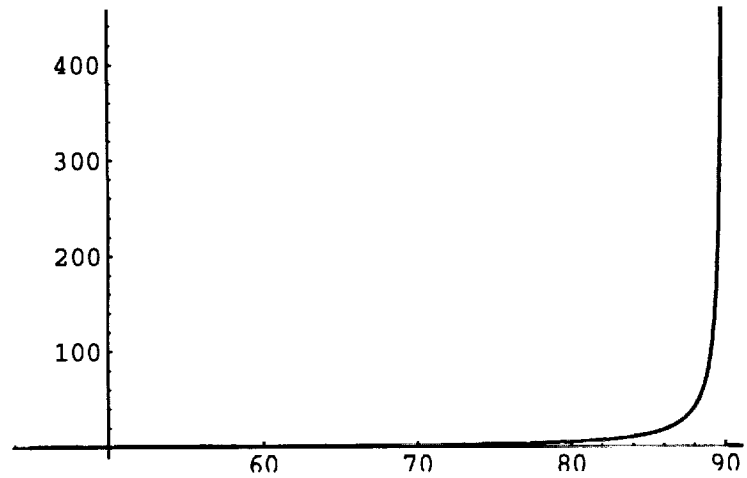


```
-Graphics-
```

```
dp[0,90,10 meter,12/2 inch]
```

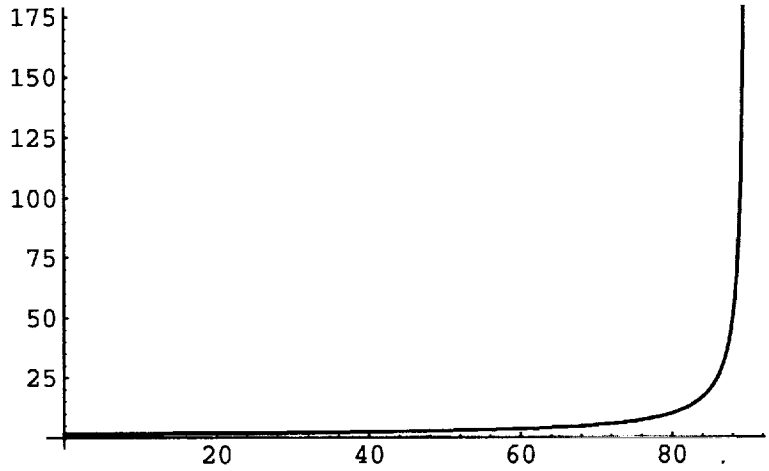


```
-Graphics-
```

```
dp[0,90,10 meter,30/2 inch]
```

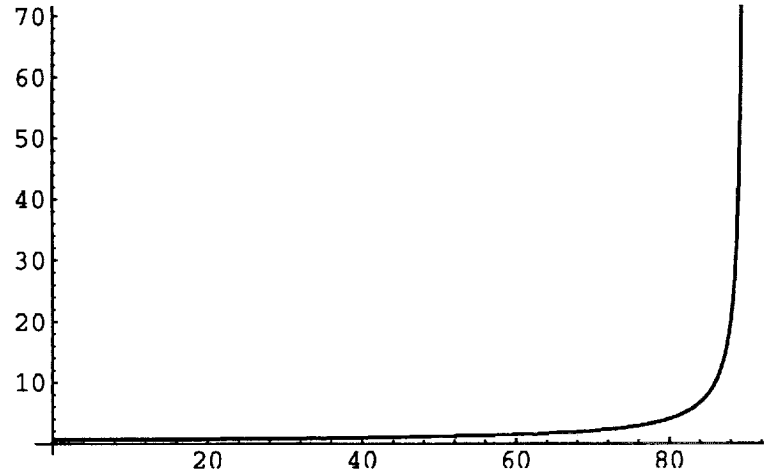


```
-Graphics-
```

In the following plots, the vertical is the smallest angle in degrees which is noticable. The horizontal axis is the angle θ shown in the figure.

```
dp1210=dp[0,80,10 Meter,1 foot];
dp310=dp[0,80,10 Meter,3 inch];
dp12100=dp[0,80,100 Meter,1 foot];
dp3100=dp[0,80,100 Meter,3 inch];
```

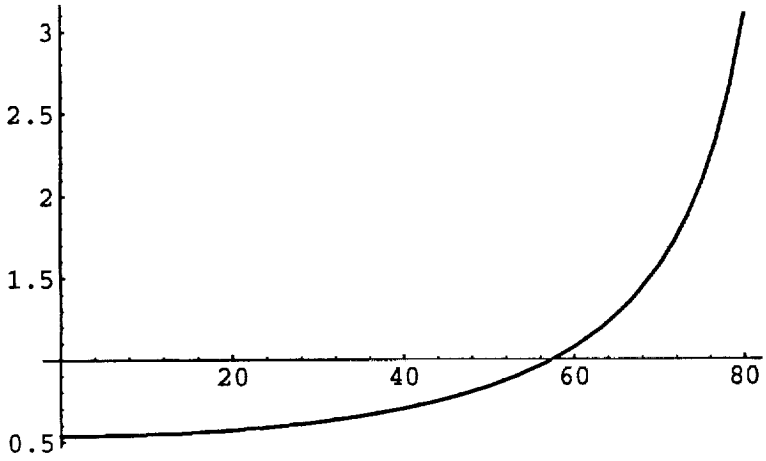

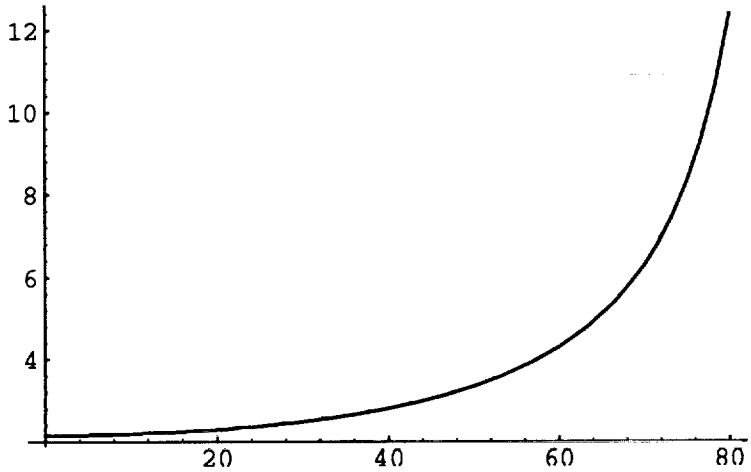

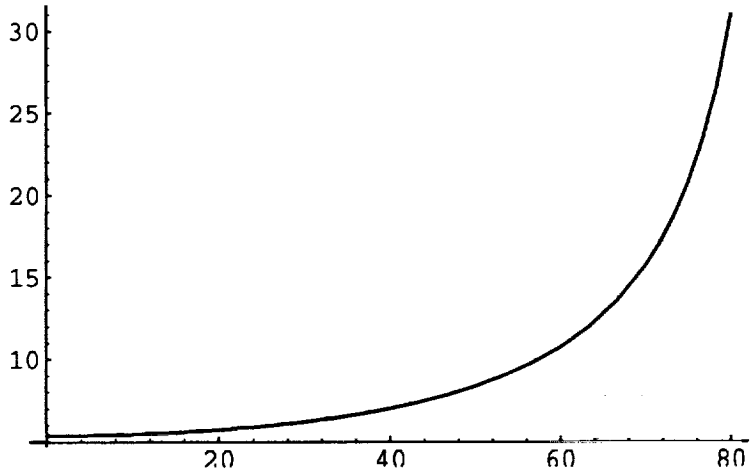

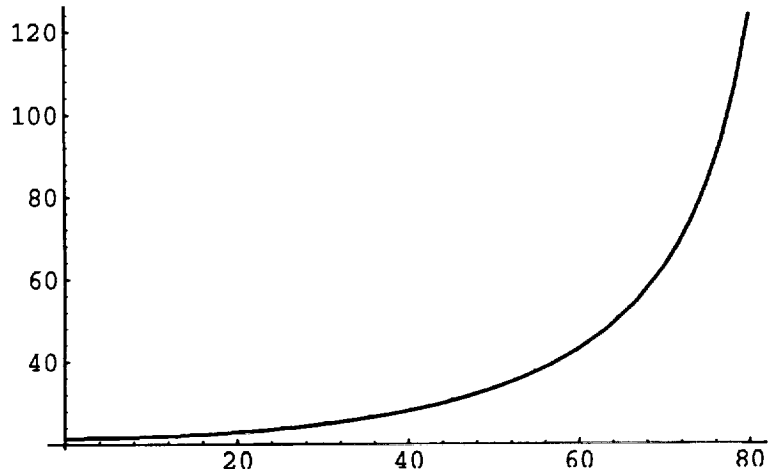

The following figure shows all four of the plots above on a single axis.

```
Show[dp310,dp3100,dp1210,dp12100]
```

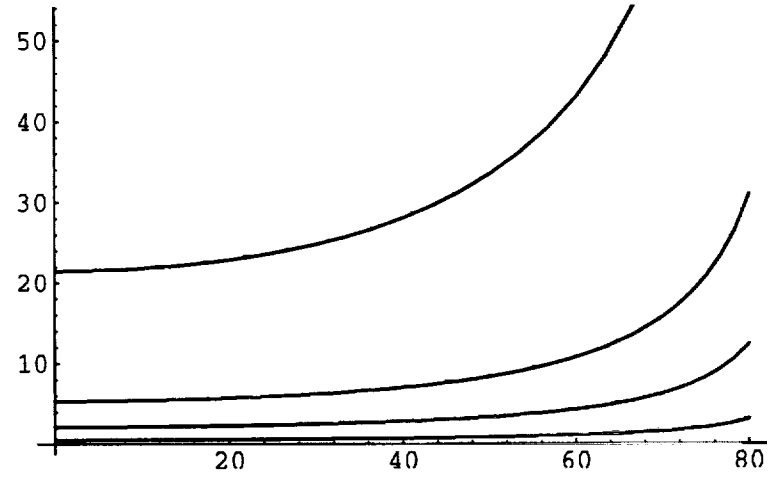


```
-Graphics-
```

Here is the equation I derived by hand.

```
dthetaperpixel[d_,l_,t_,f_]:=Block[{c,s,a,grp,grptwo},
        a=t*Degree;
        c=Cos[a];
        s=Sin[a];
        grp= 1/(d+l*c) + 1/(d-l*c);
        grptwo = (1/(d+l*c)^2 -1/(d-l*c)^2);
        value = f*l*c*grp + f*l^2*s^2*grptwo;
        Return[pixel/value]
        ];
dp[min_,max_,d_,l_]:=Plot[dthetaperpixel[d,l,x,focallength]/.{Meter->1},{x,min,max}]
```

Fourier Signal Processing.

Suppose we have a voltage coming from the PSD which is given by f.

```
f = 2Cos[t+.1] + 4 Cos[2t+1] + 6Cos[4t+.3] + 8 Cos[5t+.7];
```

This voltage looks like the following.

```
pp = Plot[f,{t,0,2 Pi}]
```

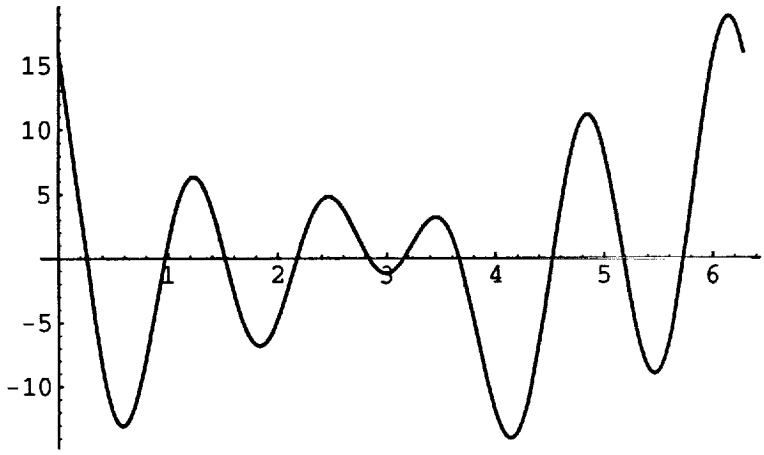


```
-Graphics-
```

Now suppose we sample the voltage beginning at t=0 for M samples. The period of our sample is the period of the slowest signal divided by M.

```
M = 16;
Period = 2 Pi;
SamplePeriod := Period/M;
```

The sample k voltage can be found from: (This is f evaluated at time = (k-1) X SamplePeriod.

```
fk[k_] := f/.t->((k-1) SamplePeriod)
```

The M sampled votages will look like:

```
ListPlot[Table[fk[k]//N,{k,1,M}],PlotJoined->True]
```

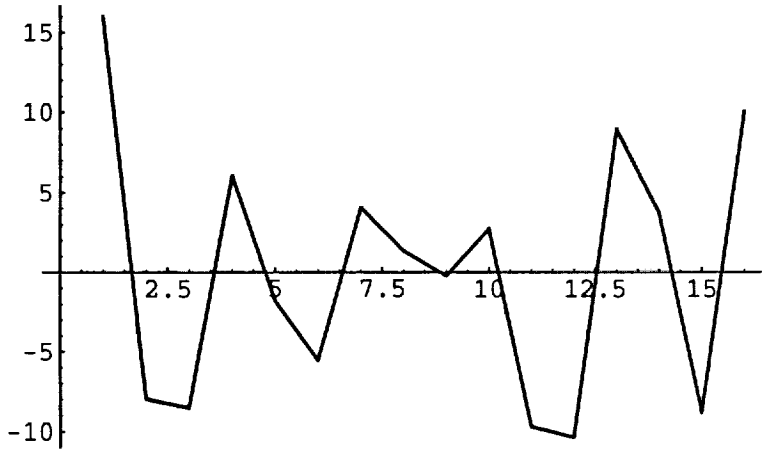


```
-Graphics-
```

If we calculate the Discrete Fourier Transform as

```
Fs[s_] := 2/M Sum[fk[r] Exp[-2 Pi I (r-1)(s-1)/M],{r,1,M}]
```

Then the Fourier cooefficients are found to be:

```
b = MatrixForm[Table[Fs[s],{s,1,M}]//N]
```

6.66134×10^{-16}

$1.99001 + 0.199667\ I$

$2.16121 + 3.36588\ I$

$-4.44089 \times 10^{-15} - 4.10783 \times 10^{-15}\ I$

$5.73202 + 1.77312\ I$

$6.11874 + 5.15374\ I$

$2.22045 \times 10^{-15} + 2.66454 \times 10^{-15}\ I$

$0. + 8.88178 \times 10^{-16}\ I$

-1.11022×10^{-16}

$0. - 8.88178 \times 10^{-16}\ I$

$2.22045 \times 10^{-15} - 2.44249 \times 10^{-15}\ I$

$6.11874 - 5.15374\ I$

$5.73202 - 1.77312\ I$

$-4.44089 \times 10^{-15} + 4.10783 \times 10^{-15}\ I$

$2.16121 - 3.36588\ I$

$1.99001 - 0.199667\ I$

The magnitude of the cooefficients is:

```
mag = MatrixForm[Table[Abs[b[[1,i]]],{i,1,M}]]
```

```
6.66134 10^-16
2.
4.
6.04944 10^-15
6.
8.
3.46845 10^-15
8.88178 10^-16
1.11022 10^-16
8.88178 10^-16
3.30093 10^-15
8.
6.
6.04944 10^-15
4.
2.
```

Notice how the magnitudes of each frequency appear?

```
realpart = MatrixForm[(b + Conjugate[b])/2];
imagpart = MatrixForm[I(b - Conjugate[b])/2];
```